Accepted: 17 October 2020
Alexandra Germain, Nathan Young, Jean-Michel Lemieux, Ariane Locat, Hugo Delottier, Philippe Fortier, Serge Leroueil, Pascal Locat, Denis Demers, Jacques Locat, and Catherine Cloutier.
Hydrogeology of a complex Champlain Sea deposit (Quebec, Canada): implications for slope stability.
Canadian Geotechnical Journal. 58(11): 1611-1626. https://doi.org/10.1139/cgj-2020-0500

Hydrogeology of a complex Champlain Sea deposit (Quebec, Canada): Implications for slope stability

Alexandra Germain[1], Nathan Young[1], Jean-Michel Lemieux[1*], Ariane Locat[2], Hugo Delottier[1], Philippe Fortier[1], Serge Leroueil[2], Pascal Locat[3], Denis Demers[3], Jacques Locat[1], Catherine Cloutier[4]

1. Département de géologie et de génie géologique, 1065 avenue de la Médecine, Université Laval, Québec (Québec), Canada, G1V 0A6.

2. Département de génie civil et des eaux,1065 avenue de la Médecine, Université Laval, Québec (Québec), Canada, G1V 0A6.

3. Section des mouvements de terrain, Direction de la géotechnique et de la géologie, Ministère des Transports du Québec, Québec, (Québec), Canada

4. Secteur Mécanique des roches, Direction de la géotechnique et de la géologie, Ministère des Transports du Québec, Québec, (Québec), Canada

*Corresponding author: jmlemieux@ggl.ulaval.ca

Abstract

The thick sequences of marine clayey deposits which blanket the St. Lawrence Lowlands in south-eastern Canada are highly susceptible to landslides. With 89% of the population of the Province of Quebec living in this region, improving our understanding of the mechanisms causing landslides in these sediments is a matter of public security. To accomplish this goal, instruments were deployed at a field site in Sainte-Anne-de-la-Pérade, Quebec, Canada to monitor atmospheric, soil, and groundwater conditions. Field and laboratory measurements of soil geotechnical and hydraulic properties were also performed. Results indicate that the groundwater and pore pressure dynamics at the site cannot be explained using simplified site conceptual models. Further analysis indicates that groundwater dynamics and pore pressures in the massive clay deposits on-site are determined by (i) the highly-heterogeneous nature of the local geological materials (ii) the contrasting hydraulic and geotechnical properties of these materials, (iii) the presence of two unconfined aquifers at the site, one surficial and one at depth, and (iv), the presence of the Sainte-Anne River. These results were used to create a new conceptual model which illustrates the complex groundwater flow system present on site, and shows the importance of including hydrogeologic context in slope stability analysis.

Keywords:

1 Introduction

Landslides in sensitive clays represent one of the largest geological hazards in Eastern Canada (Hungr and Locat 2015; Locat et al. 2017). The St. Lawrence Lowlands, located primarily in south-eastern Quebec, are composed of thick, landslide-prone clayey sediments that were deposited as post-glacial seas inundated the area at the end of the Wisconsin glaciation (Parent and Occhietti, 1988). In the province of Quebec, 80% of reported landslides are located within the boundaries of these ancient seas (Demers et al. 2008). Furthermore, as 89% of the population of the province lives in the area of the ancient Champlain, Laflamme, and Goldthwait seas, improving our understanding of the mechanisms that trigger landslides in these sensitive clays is a matter of public security (Demers et al. 2014).

The properties of sensitive clays, as well as landslides occurring in these materials, have been a topic of intensive study since the 1970s (Jarrett and Eden 1970; Lafleur and Lefebvre 1980; Tavenas 1984; L'Heureux et al. 2014; Lefebvre 2017). In the St. Lawrence Lowlands, land emergence following deglaciation resulted in the development of groundwater flow conditions which promoted the leaching of the salts in the marine sediments. Previous work has demonstrated that this leaching results in a decrease in the liquid limit of the sediments, resulting in the generation of highly sensitive clays (Torrance 1975; Locat et al. 1984). The concurrent formation of a drainage network on the former sea floor resulted in the initiation of slope formation and mass wasting processes, such as landslides (Quigley 1980; Locat 1996; Locat et al. 2003). Today, slope instabilities are generally related to both the role of pore pressure variations (e.g. snowmelt, intense rainfall), erosion (riverine or coastal) and occasional earthquakes (Rosenberg et al. 1985; Locat 2011; Gauthier and Hutchinson 2012, Cloutier et al. 2016; Uhlemann et al. 2016).

Due to the effects of climate change, site assessments that only consider a single set of static conditions may not be sufficient for forecasting future landslide risk. Recent work has shown that in many landslide-prone regions, shifting temperature and precipitation patterns are likely to alter subsurface flow regimes and pore pressure distributions (Boyle et al., 2009; Comenga et al. 2013). In South-Eastern Quebec, a shift in precipitation type from snow to rain during the winter is projected to decrease the magnitude of the spring snowmelt event by 10% (Cloutier et al. 2016). This shift could cause a decrease in landslides during the spring, as a decreased snowmelt could result in a reduction of the magnitude and duration of elevated pore pressures during this period (Lefebvre and Lafleur 1978). However, increased rainfall during other seasons, particularly winter, is likely to alter slope stability and landslide timing in ways that are not currently well understood.

The present study is part of a major inter-agency effort focused on understanding potential changes in climatic conditions, and the effects such changes could have on landslide activity in Quebec. As part of this effort, a series of instrumented sites representing various morphological conditions were established, and data from one such site is reported herein (Cloutier et al. 2017).

The Sainte-Anne-de-la-Pérade site presented here was selected to evaluate water infiltration and pore pressure variations. To ensure one-dimensional conditions for groundwater flow analysis, the site was located at a distance sufficiently remote (450 m) from the slope scarp near the river (e.g., a Type 2 site, Cloutier et al. 2017; Figure 1). Interestingly, due to the complexity of the local stratigraphy and river morphology, the detailed analysis of the infiltration and groundwater flow shown below indicates that the 1-D hypothesis does not apply here. Instead, the analysis provides a clear example of local hydrogeological conditions which differ greatly from those present at the sites of previous slope-stability analyses conducted in sensitive clays in Quebec (e.g., Lafleur and Lefebvre 1980; Lefebvre 2017).

To perform this investigation, an extensive array of instrumentation was deployed at a site in Sainte-Anne-de-la-Pérade to monitor atmospheric, soil, and groundwater conditions at a high temporal and spatial resolution. Measurements of soil geotechnical and hydraulic properties were conducted in the field, and soil samples were collected for further laboratory analysis. The paper is organized as follows: first, the study site is presented, followed by descriptions of the soil characterization program, the instrumentation, and the methods of interpretation. Soil properties, transient soil water conditions, and associated infiltration and groundwater flow dynamics are then presented in detail. A discussion focusing on the implications of the hydrogeological context, infiltration dynamics, and the impact of groundwater flow conditions on slope stability then concludes the analysis.

2 Study Area and Instrumentation

The study area is located in Sainte-Anne-de-la-Pérade, a municipality roughly 100 km to southwest of Quebec City, within the St. Lawrence Lowlands basin (Figure 1a). The area of investigation is located on the western bank of the Sainte-Anne River, a major tributary of the St. Lawrence River, where many landslides occur every year. The field site is an area of level terrain located approximately 450 m from the Sainte-Anne River and away from any slopes with active erosion (Figure 1b, red square). After the site was instrumented and initial data were analyzed, the complexity of the flow conditions found on-site necessitated expanding the study area to include a more regional context. As a result, the study area was extended across a 2 km^2 area, and additional hydraulic data were gathered from piezometers that were already in place (Figure 1b, circles).

2.1 Study Area

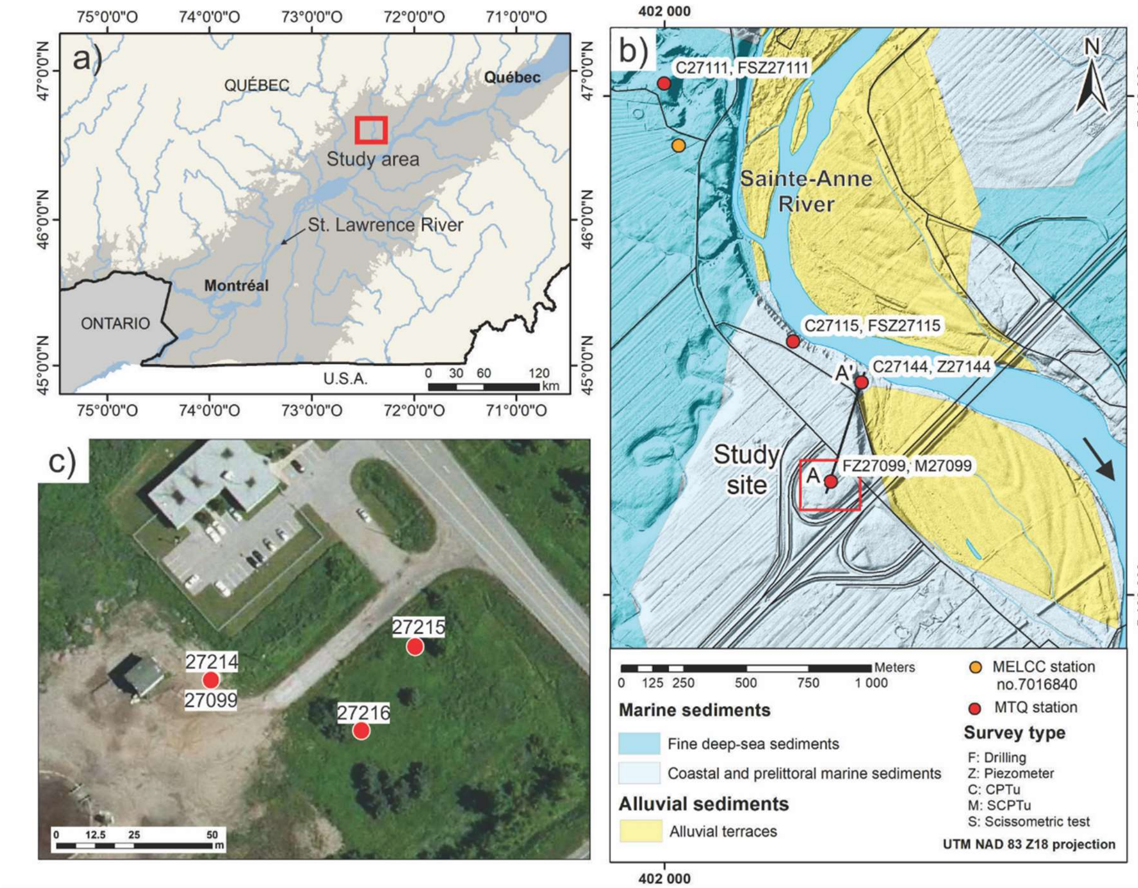

Figure 1. a) Location of the study area in the St. Lawrence Lowlands showing the area inundated by Champlain Sea (dark gray). b) Digital elevation model and surficial geology map of the study area showing the location of the study site and available data. c) Map of the study site showing the location of instruments.

The bedrock underlying the study area is the Utica Shale of the St. Lawrence Lowlands basin, and is primarily composed of calcareous shale and clay limestone. The sediments of the study area are commonly characterized as a thick clay plain, where the deep water marine sediments (clay) are locally overlain with littoral deposits (Figure 1b). Alluvial deposits are found locally along the Sainte-Anne rivercourse. The Sainte-Anne river is deeply incised, and the steep slopes lining both the river and its minor tributaries are marked by scarps from several previous landslides (Figure 1b).

While the study site stratigraphy was first presented by Diène (1989), an additional 37-m-deep borehole (27099, Figure 1c) was drilled and cored for this study (Figure 2). The core log showed a complex geologic setting composed of sediments underlain by shale and limestone (BR). Overlying the shale is a layer of till (T), followed by thick silt and clay deposits with traces of sand that span over 10 metres (LSC). The silt is overlain with a silty sand layer (2 m thick), followed by a fine sand layer with traces of clay (4 m thick). These two units are hydrostratigraphically similar, and are combined into the hydrostratigraphic unit Sd_L (6 m thick). Above unit Sd_L is a 4.5-m-thick silt unit with layers of fine sand (SLS). This unit is followed by an 8-m-thick layer of silty clay (USC). The upper 3 m of the site is composed of a complex succession of fine and medium sand overlain by fine sand with silt lenses (these layers are combined in the hydrostratigraphic unit Sd_U and a detailed stratigraphic description is provided below). This unit is then capped by a layer of clayey silt, which forms the modern surficial material (MS). The water table is found in the unit Sd_U, about 2.1 m below the ground surface.

A piezocone test with pore-water pressure measurement (CPTu) was conducted adjacent to the cored borehole (27099 location, Figure 1c). The CPTu gives continuous, detailed information on the stratigraphy of the site (corrected tip resistance, q_t; water pressure, u; and sleeve friction resistance; Figure 2). A 600 m conceptual cross-section (line A-A', Figure 1b) was prepared using the borehole and CPTu data in order to show the continuity of sediment units between the study site and the Sainte-Anne River (Figure 3). The orientation of the units was corroborated by core logs taken from site 27115, located approximately 500 m to the north (Figure 1), and the results presented in Diène (1989). The sand units shown in Figure 3 are not regionally continuous, but were also identified in the core logs from site 27115. Thus, for the purposes of the analysis presented here, the sand units are assumed to be continuous over the study area, while unit Sd_L outcrops at the Sainte-Anne River elevation.

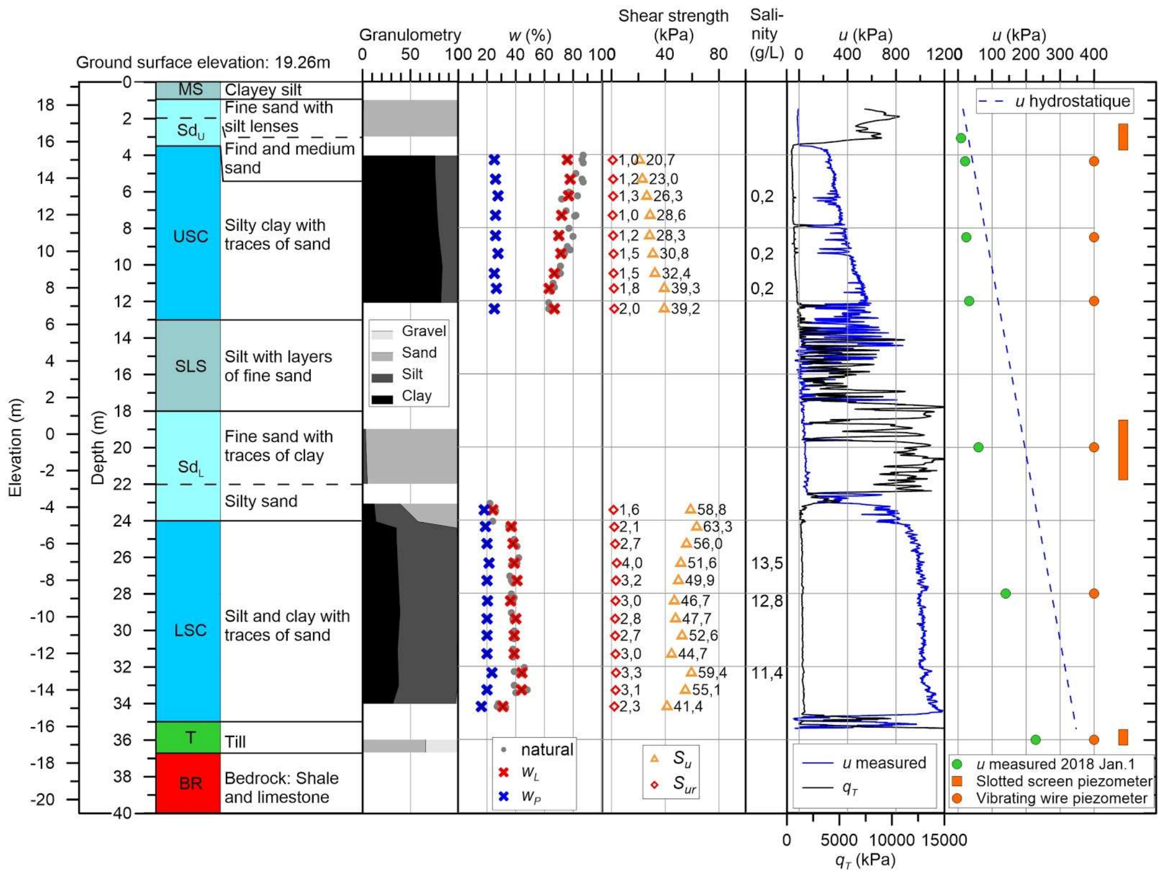

Figure 2. Geotechnical profile at Location 27099 (located on Figure 1c) showing site stratigraphy, granulometry, liquid and plastic limits, undrained shear strength, pore-water salinity, pore pressure and corrected tip resistance from CPTu, pore pressure measurement with VWP and slotted-screen piezometers.

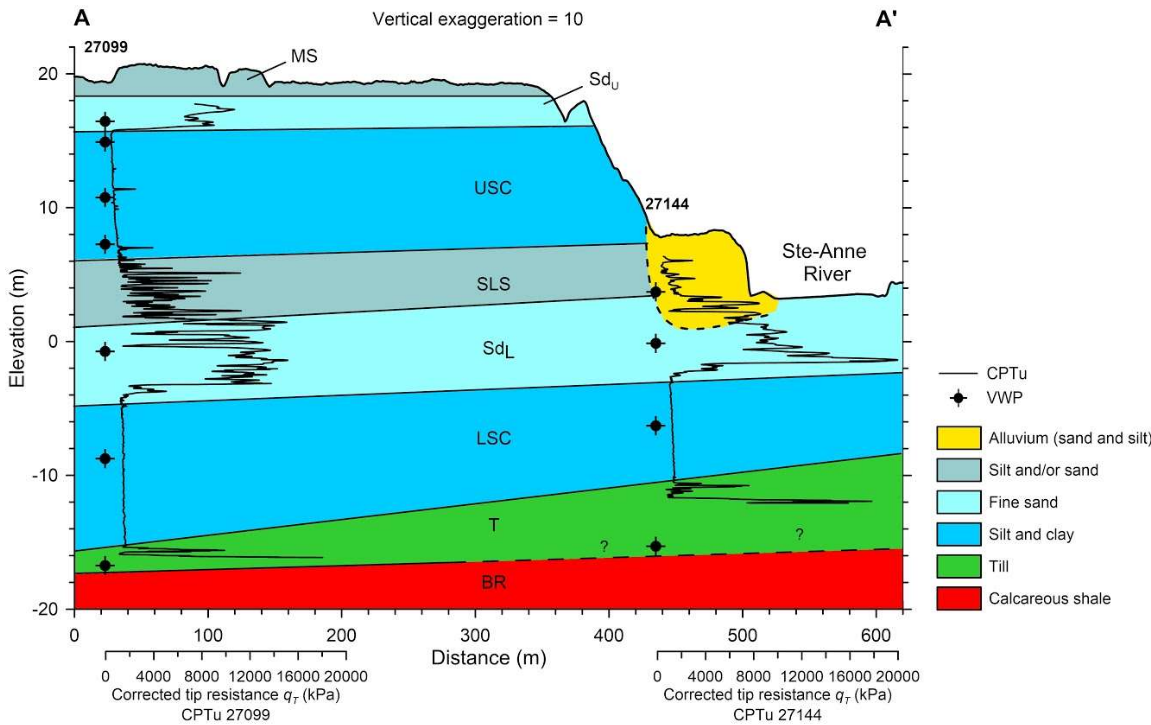

Figure 3. Cross-section across the study area (located on Figure 1b) showing the continuity of sedimentary units and corrected tip resistance used for the interpolation of unit contacts.

2.2 Instrumentation

Instrumentation at the Sainte-Anne-de-la-Pérade site monitored weather, soil (unsaturated zone) and groundwater (saturated zone) conditions, from Spring 2017 onward. These were deployed at four locations,identified by the following numbers according to MTQ nomenclature: 27099, 27214, 27215, 27216 (Figure 1c Cored boreholes, cone penetration tests, multilevel piezometer nests and a governmental weather station (located 1.2 km away from the study site) were also used for this study (Figure 1b).

A local weather station (installed at Location 27216 in late summer 2017) measured precipitation, barometric pressure, solar radiation, wind direction and speed, snow thickness, air temperature and relative humidity on an hourly basis. Probes were installed in the unsaturated zone beside the local weather station to monitor water infiltration and the soil thermal regime (Figure 4). Thermistors (RocTest, TH-T), water content probes (METER, 5TM) and tensiometers (METER, MPS-6) were used to monitor infiltration between depths of 2.5 cm and 2 m (Figure 4).

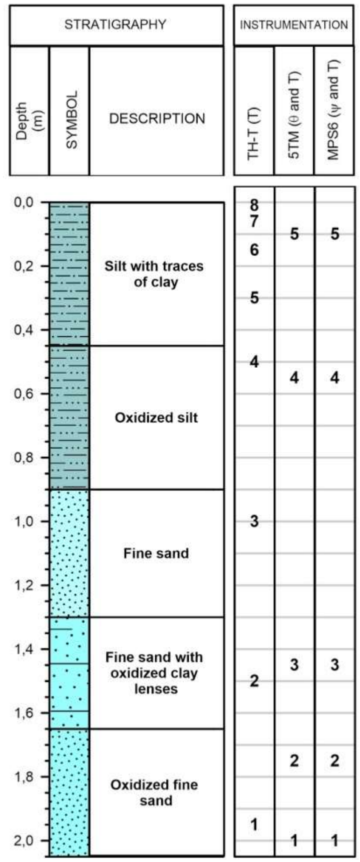

Figure 4. Instrument depth and the geological units in which they are located (Location 27216). Numbers in the right part of the figure refer to the probe number.

Hydraulic heads in the saturated zone were monitored with two types of piezometers: buried vibrating-wire piezometers (VWP; Geokon 4500S) and slotted-screen hydraulic piezometers. Four VWP were arranged in a multilevel configuration (depths = 4.5, 8.5, 12 and 20 m) using sand packs and bentonite plugs, while the other two VWP were stand-alone installations (depths = 28 and 36 m) that used sand packs and bentonite plugs (Figure 2). Three 5.08-cm-diameter slotted-screen PVC piezometers (slot size 10) were also deployed at each location in the coarse grain units (Sd_U, Sd_L and T, at depths of 3, 20 and 36 m, respectively), to measure hydraulic conductivity with slug tests, determine groundwater flow directions, and the hydraulic gradient (Locations 27214, 27215 and 27216, Figure 1c). These nine wells were equipped with leveloggers (Solinst 3001). Installation depths and screen lengths for the hydraulic piezometers are shown in Figure 2.

3 Methodology

This section presents the methods used to measure the geotechnical and hydraulic properties of the soil and perform the barometric compensation. The simple analytical equation used to model groundwater flow dynamics at the site is also described.

3.1 Geotechnical and Hydraulic Properties

3.1.1 Geotechnical properties

The geotechnical properties of cohesive soils were determined using shelby tube samples, while a split-spoon sampler was used to collect samples of the coarse-grained materials. A Swedish cone penetrometer was used on cohesive samples from each unit to obtain the undrained shear strength (S_u), remoulded undrained shear strength (S_{ur}), and liquid limit (w_L) using the CAN/BNQ 2501-110 standard methods. The plastic limit (w_P) and natural water content (w) were also measured at several elevations. Pore-water salinity was assessed by extracting the pore-water from the samples through the application of pressure, then measuring the conductivity of the resulting effluent. Particle size analysis using sedimentometry was performed using the CAN / BNQ 2501-025 standard methods. Particle size analysis of the coarse materials (Units Sd_U and Sd_L; Table 1) was performed with sieves and sedimentometry.

3.1.2 Hydraulic properties

Hydraulic properties were determined from laboratory and field tests.

Vertical hydraulic conductivity measurements for units USC and LSC were obtained in triaxial cell on samples from depths of 6.14, 9.28, 11.19, 26.24, 28.19 and 32.13 m under confining stresses in the overconsolidated range. This technique was used as it allows for larger sample volumes than those used for oedometric tests. Thus, the resulting hydraulic conductivity values should be less affected small-scale heterogeneities and more closely approximate *in situ* values.

In addition to the laboratory measurements, a 45-day pumping test was performed from 22/06/2018 to 06/08/2018 in Unit Sd_L to obtain the *in situ* vertical hydraulic conductivity of the USC unit above. The pumping test was conducted in a 2-inch diameter pumping well (27215, Figure 1) with an extraction rate of 8 litres/minute. All piezometers on site were used as monitoring wells. The results of this pumping test are not presented here as it did not induce any drawdown in the USC unit, but the effects of the pumping can be seen in some of the piezometric data analyzed in this study.

The hydraulic conductivity of the coarse-grain layers (Units Sd_L, Sd_U, and T), was determined by conducting slug tests in the 9 slotted-screen piezometers located on site. The data from tests conducted in the unconfined aquifers (Units Sd_U and Sd_L) were analyzed using the method of Bouwer and Rice (1976). For the confined aquifer (Unit T), the method of Cooper et al. (1967) was used. More details on the slug tests performed on site is provided in Fortier et al. (2018).

3.3 Barometric compensation

Barometric compensation was performed on the piezometer data to correct for variations in atmospheric pressure. For the slotted-screen piezometers, a simple correction was performed by removing the atmospheric pressure values from the total pressure measured by the levelogger. For the vibrating-wire piezometers, observed variations in atmospheric pressure are dependent on the compressibility of the soil unit containing the piezometer. While there are many methods for correcting data from VWPs, this study used the linear regression method, as it is both robust and relatively easy to apply (Marefat et al. 2015; Tipman et al. 2017):

$$u_t^* = u_t - LE(B_t - B_{ave}) \tag{1}$$

where: u^* is corrected pore pressure [kPa], u is the raw pore pressure, measured with the vibrating wire piezometers [kPa], LE is the barometric loading coefficient, B is the measured atmospheric pressure [kPa], B_{ave} is the mean atmospheric pressure measured during the period of investigation [kPa] and t is the time of measurement.

In Equation 1, the loading efficiency (LE; which depends on the soil compressibility), must be obtained before applying the barometric compensation. For undrained conditions, LE can be computed from the slope of the linear relationship between observed pore pressure changes and barometric changes, assuming that barometric pressure is the sole cause for pore pressure changes (Marefat et al. 2015):

$$LE = \frac{\partial u_w}{\partial B} \tag{2}$$

In this study, only data from the winter period were used to determine LE, as the ground is frozen and covered with snow at this time. Thus, data from this period will likely comply with the assumption of Marefat et al. (2015) that any observed variations in water pressure are directly attributable to barometric variations.

Variables obtained through the application of barometric compensation further allow for computation of the vertical compressibility and the specific storage coefficient (Freeze and Cherry 1979; Marefat et al. 2015):

$$m_v = \frac{(LE n \beta_w)}{(1-LE)} \tag{3}$$

$$S_s = p_w g(n\beta_w + m_v) \tag{4}$$

where m_v is vertical compressibility [Pa^{-1}], n is porosity [D], β_w is the compressibility of water at 20°C [Pa^{-1}], S_s is specific storage [m^{-1}], ρ_w is the unit mass of water [$kg \cdot m^{-3}$], and g is the acceleration due to gravity [$m \cdot s^{-2}$].

The specific storage coefficient is then used to compute hydraulic diffusivity, D [m^2/s], which is proportional to the speed at which a finite pressure pulse propagates in the flow system (Freeze and Cherry 1979):

$$D = \frac{K}{S_s} \tag{5}$$

3.4 Groundwater flow modelling

To better understand the observed hydraulic head variations at the study site, a simple analytical solution was used to model two different flow systems. While more complex and rigorously-documented analytical solutions exist (e.g., the step-response functions of Moench and Barlow 2000) the purpose of the modeling presented here was to assess whether changes in river stage could be a possible explanation for the hydraulic behavior observed at the study site. Thus, the results of these simple analytical solutions represent cursory investigation into the dynamics of the field site, as opposed to a rigorous attempt to quantify the contribution of specific physical processes to the measured pore pressure distributions. Therefore, despite the fact that the solutions used here are not completely appropriate for the observed conditions (i.e., not exclusively 1-D, partially unsaturated), they do provide some insight into the dynamics of the local flow system, and can help guide future work with more complex analytical solutions or numerical models.

First, vertical downward flow from the surface aquifer into unit USC was considered to assess whether downward groundwater flow at the site could explain the pore pressure observations in the piezometers. Since the conceptual cross-section presented in Figure 3 demonstrates that unit Sd_L is continuous up to the Sainte-Anne River, a second simulation was conducted with the same analytical solution to examine the impact of the horizontal propagation of pore pressures. This second simulation examined whether pore pressure increases detected on-site were the result of river-stage-driven variations pore pressure propagating horizontally in unit Sd_L.

3.4.1 Vertical flow

First, an analytical solution was used to describe 1-D, transient, vertical (i.e., downward) flow within the upper clay unit (USC). The solution assumes fully saturated flow in a semi-infinite, 2-D, homogeneous and isotropic porous domain (Figure 5). The groundwater flow equation describing these conditions is given by:

$$D\frac{(\partial^2 h)}{(\partial z^2)} = \frac{\partial h}{\partial t}, z, t \geq 0 \qquad (6)$$

where h is the hydraulic head, D is hydraulic diffusivity, z is the spatial dimension and t is time.

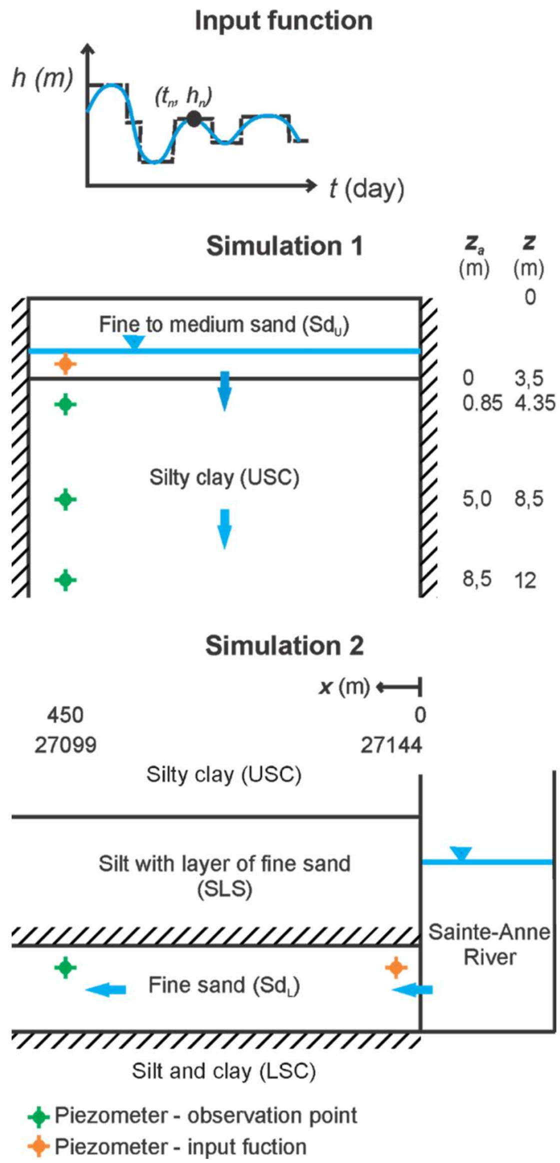

Figure 5. Diagrams illustrating the conditions of the simulations for vertical downward flow in unit USC (Simulation 1), and for horizontal flow in the unit Sd_L (Simulation 2). Both simulations use a different input function.

This equation is solved using the superposition principle in order to obtain transient hydraulic heads at various depths within the clay layer resulting from water table variations in the overlying aquifer (Figure 5 - input function). The water table variations are discretized in panels of equal length. The solution is given by (Neville, personal communication):

$$h = h_i + \sum_{n=1}^{NP} \Delta h_n ERFC \left\{ \frac{z_a}{2\sqrt{D(t - t_{sn})}} \right\} \quad (7)$$

where h_i is the initial head in the soil, NP is the number of points (panels) defining inflow head history, n is the current panel, dh_n is the change in hydraulic head from panel n-1 to n, z_a is the depth where the head is calculated, t is elapsed time since the beginning of the simulation, and t_{sn} is time at the beginning of panel n.

In this simulation, observation points in unit USC correspond to the locations of vibrating-wire piezometers at the study site (depths of 4.35 m, 8.5 m and 12 m; Figure 5). The data from these vibrating-wire piezometers are used to compare simulation results to field observations. Since unit USC begins at a depth of 3.5 m (corresponding to point 0), the depths (z_a) of the observation points are 0.85 m, 5 m and 8.5 m, respectively. The corrected water level data from Well 27214 at 3 m depth was used to represent the initial hydraulic head and the hydraulic head at time n. The simulation is carried out for a period of 170 days since 01/03/2018 with 12-hour time steps.

3.4.2 The influence of the Sainte-Anne River

A second model was constructed to test the idea that observations from the piezometers in the lower sand unit (Sd_L) reflect the propagation of a pressure wave resulting from changes in the stage of the Sainte-Anne river. While Equation 7 was also used for this simulation, the resulting hydraulic head varies with horizontal distance from the river, as opposed to depth (Figure 5). The same assumptions from Equation 7 are utilized, but certain parameters were modified: horizontal distance, x, was used in place of z_a, and the hydraulic diffusivity value was changed to reflect the properties of sand, instead of silty clay. Various values were used until the best visual fit to the data was obtained.

The propagation distance of the pressure wave corresponds to the distance between the Sainte-Anne river and Location 27099 of the study site, approximately 450 m. In this simulation, data from the VWP at 20 m depth were used to compare the simulated results with field observations at Location 27099. The prescribed hydraulic heads at the inflow boundary correspond to variations in the water level of the Sainte-Anne River. However, since variations in the level of the river near the site are not known, the data from the VWP closest to the river level (Location 27144, 7.84 m depth), are used. The simulated heads are also compared to river discharge observations recorded by a gauging station approximately 50 km to the north. The simulation is carried out for a period of 170 days beginning on 01/03/2018 with 12-hour time steps. During the period of the simulation, the river was not influenced by flooding or ice jamming.

4 Results

In this section, the geotechnical and hydraulic properties obtained from field and laboratory investigations are presented first. These results are followed by climate and unsaturated zone monitoring data, which are later used to explore infiltration dynamics at the study site. Finally, hydraulic head data are presented, along with the results of the analytical models.

4.1 Geotechnical and hydraulic properties

4.1.1 Geotechnical properties

Particle size measurements were performed on most of the units. Results of this analysis allowed us to divide the deposit into distinct units (from bottom to top: T, LSC, Sd_L, SLS, USC, Sd_U and MS) as shown in Figure 2. Particle size data of the clay units show that unit LSC is composed of an average of 62% of silt, 36% of clay and about 1% sand, while unit USC is composed of an average of 79% clay, 21% silt and 0.3% sand. The till (T) consists mainly of sand and gravel.

The natural water content w of the LSC unit is around 40% and is constant throughout the unit (Figure 2). In unit USC, the natural water content increases from 65%, at the bottom of the unit, to 85%, near the top. The plastic limits (w_P) in units USC and LSC are very similar: close to 20% for unit LSC, and 25% for unit USC. Unit LSC has a liquid limit (w_L) around 40%, a value close to the natural water content. Unit USC has a higher w_L value than unit LSC, increasing from 65% at the bottom of the unit, to 75%, at the top of the unit. The plasticity index I_p in unit LSC has a fairly consistent value close to 20, unlike the surficial layer of silty clay, unit USC, where it varies from 37 to 52. The liquidity index (I_L) is around to 1 in the LSC and increases from 1, at the bottom of the unit, to 1.2, at the top of the unit.

The intact undrained shear strength (S_u), from fall cone tests performed in units LSC and USC, gradually increases with depth, from 41.4 to 63.3 kPa for LSC and from 20.7 to 39.2 kPa and USC, respectively (Figure 2). The undrained remolded shear strength values (S_{ur}) ranges from 1.6 to 2.3 kPa in unit LSC and from 1 to 2 kPa, giving sensitivity values ($St = S_u/S_{ur}$) varying from 18 to 37, from bottom to top of unit LSC, and from 19 to 21, from bottom to top in unit USC. These values are consistent with the liquidity index mentioned above. Pore-water salinity varies between 11.4 and 13.5 g/L for LSC, however a constant value equal to 0.2 g/L was found in unit USC (Figure 2), indicating leaching of the unit. LSC and USC are therefore respectively stiff and firm clay with a medium sensitivity, properties common to Eastern Canadian sensitive clays (Leroueil et al. 1983).

The corrected peak resistance (q_T) and pore pressure u as a function of depth, obtained by the CPTu, make it possible to clearly visualize the contacts between the different layers of sediment present on site (Figure 2). The lower resistances with increasing pore pressure correspond to more clay-rich, lower-permeability layers, such as units LSC and USC, while the higher resistances and decrease in pore pressure correspond to layers more permeable layers with higher sand contents, such as SLS and Sd_L. In addition, the CPTu profile indicates the presence of stratification in the lower units.

Pore pressures measured with vibrating-wire piezometers in unit USC show that the *in situ* values are lower than hydrostatic conditions, suggesting groundwater flow towards the base of the massive clay layers (Figure 2). However, within the units below USC, the hydraulic gradient is either hydrostatic or very close to hydrostatic.

4.1.2 Hydraulic properties

For the two massive clay units (LSC and USC), the vertical K_v values are in the range of 10^{-9} to 10^{-10} m/s, which corresponds to the values found in the literature (Leroueil et al. 1983; Tavernas et al. 1983; Table 1). This also compares well with the values obtained from Diène (1989) for the USC unit using an *in situ* permeameter and piezometers with various lengths (0.5 to 5.5 $\times 10^{-9}$ m/s). The hydraulic conductivities of both clay units (USC and LSC) are similar, with unit USC having a geometric mean K_v of 6.4×10^{-10} m/s and unit LSC having a value of 8.7×10^{-10} m/s. For the coarser grain materials present on site (i.e., units Sd_U, Sd_L, and T) the geometric mean K_H values measured were 3×10^{-7}, 9.8×10^{-6} and 3.8×10^{-5} m/s for units T, Sd_L, and Sd_U, respectively (Table 1).

Table 1. Hydraulic and poroelastic properties for materials sampled on site.

Sediment Type (Unit)	Interval (m)	Piezometer depths (m)	Triaxial cell sample depths (m)	Vertical K (m/s)	Geometric mean horizontal K (m/s)	*n*	S_s (m^{-1})	*LE*	m_v (kPa^{-1})
Clayey silt (MS)	0.0 – 0.9	-	-	1.4×10^{-6}	-	0.45	-	-	-
Fine and medium sand (Sd_U)	0.9 – 3.5	2.8	-	-	3.8×10^{-5}	0.33	-	1.27	-
Silty clay (USC)	3.5 – 13	4.4	6.09 – 6.19	4.5×10^{-10}	-	0.69	1.0×10^{-4}	0.97	1.0×10^{-5}
		8.5	9.22 – 9.33	1.1×10^{-9}		0.67	3.8×10^{-5}	0.92	3.5×10^{-6}
		12.0	11.13 – 11.24	5.3×10^{-10}		0.63	3.6×10^{-5}	0.92	3.3×10^{-6}
Fine sand (Sd_L)	18.0 – 24.0	20.0	-	-	6.9×10^{-6}	0.37	2.5×10^{-6}	0.32	8.0×10^{-8}
Silt and clay (LSC)	24.0 – 35.0	28.0	26.19 – 26.28	8.5×10^{-10}	-	0.50	6.3×10^{-6}	0.64	4.1×10^{-7}
			28.14 – 28.24	1.1×10^{-9}					
			32.08 – 32.18	7.1×10^{-10}					
Till (T)	35.0 – 36.7	36.0	-	-	3.0×10^{-7}	0.42	2.5×10^{-6}	0.24	6.1×10^{-8}

The vertical compressibility values of the silty clay layers (3.3×10^{-6} kPa^{-1} to 1.0×10^{-5} kPa^{-1}) and silt and clay (4.1×10^{-7} kPa^{-1}) are larger than the values in the sand and till layers (6.1×10^{-8} kPa^{-1} - 8.0×10^{-8} kPa^{-1}). Specific storage S_s results are similar to the results obtained by Marefat et al. (2015) for clays from the Champlain Sea. Overall, the finer grained units (MS, USC, LSC) have a higher compressibility and porosity, but a lower hydraulic conductivity than the sandy units (Sd_U Sd_L; Table 1).

4.2 Infiltration dynamics

During the period of study, daily mean air temperature values range from -22 °C to 28 °C. From November to June, the average temperature was 0.14°C for 2018 and 0.89°C for 2019 (Figure 6a). For the two recorded winters (2017 and 2018), the snow is accumulated from October to April. The maximum snow thickness was 0.92 m, which was recorded in March 2019 (Figure 6b). The snowmelt period is almost entirely confined to the month of April and May. Cumulative precipitation at the site, taken from September 1, 2017 to June 31, 2019 was 1589 mm (Figure 6b).

The soil data includes the water content data (5TM probes), the hydraulic heads in unit Sd_U and the soil temperatures. The water content observed by all probes increases rapidly in the spring due to snowmelt infiltration (Figure 6c). A smaller increase was recorded by 5TM probe # 4, which was expected due to its location within the low-K surficial silt unit (MS) where there is little water flow. Water content in this layer is also virtually constant throughout the year. 5TM probe # 5, located in the root zone (just above probe #4), was the most sensitive to changes in water content. Data indicate that during large liquid precipitation events, both probes register an increase in water content at the same time, however the water content measured by probe #4 decreases rapidly after the cessation of the event. Probe #4 sees fewer changes in water content in winter, as snow cover limits the amount of surface water infiltration. However, when the recorded air temperature in winter is above 0 degrees, water content measurements begin to rise, indicating that infiltration resumes quickly once liquid water is present, even in periods when the ground is frozen (e.g. January 2018). All other 5TM probes are located in unit Sd_U. Data indicate that this unit becomes saturated in the spring, as the volumetric water content measurements plateau at a value corresponding to saturation. Data further indicate that this unit drains downward throughout the summer.

The three screened piezometers in the upper aquifer (Sd_U) on site behave very similarly, as evidenced by both the synchronicity and magnitude of the observed changes in water levels (Figure 6d). Spring snowmelt represents the largest source of recharge, and infiltrating snowmelt drives water level increases of 1 to 1.7 m across the three wells. The shallowest depth of the water table measured in well 27216C during this period is about 1.5 m, which explains why some of the 5TM probes installed in the unsaturated zone observed saturated conditions.

Soil temperature data show variations between -1.4 ° C and 26.2 ° C during the period of study (Figure 6e). The depth of the zero-degree isotherm indicates that the maximum depth of frost propagation was 34 cm in 2018 and close to 40 cm in 2019.

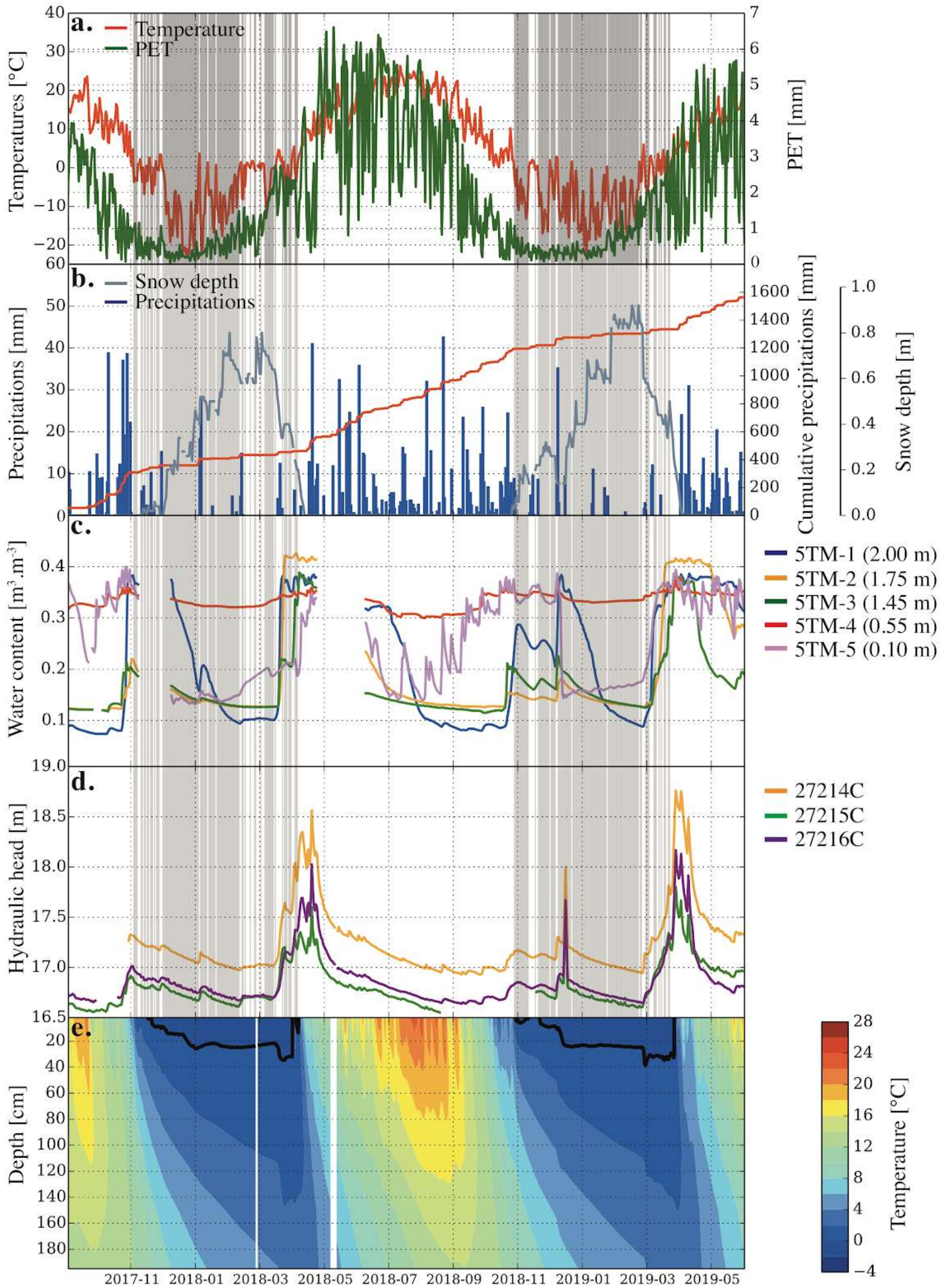

Figure 6. Weather and soil datasets at the study site. Vertical gray bands underline periods when the mean daily temperature is below 0°C. All the data has been aggregated into a daily basis. a) air temperature and potential evapotranspiration (PET) as computed from the FAO Penman-Monteith equation on an hourly basis. b) Daily and cumulative

precipitations, along with snow depth. c) Volumetric water content. d) Hydraulic head in the Sd_U unit. e) Soil temperature.

4.3 Groundwater flow

Hydraulic heads computed from compensated pore pressure data show that pore pressures (presented here as hydraulic head) increase in the spring across all VWPs (Figure 7). The amplitude of the peaks varies depending on piezometer depth, while the time lag of the peak varies as a function of depth. The high frequency component of the signal also dampens with depth. Notably, the hydraulic head of the piezometer at 20m depth varies between 4.5 and 6 m, which is below unit USC. Considering the contrast in hydraulic properties between units SLS and USC (e.g., Table 1), this observation suggests that an unsaturated zone may exist just below unit USC some time during the year.

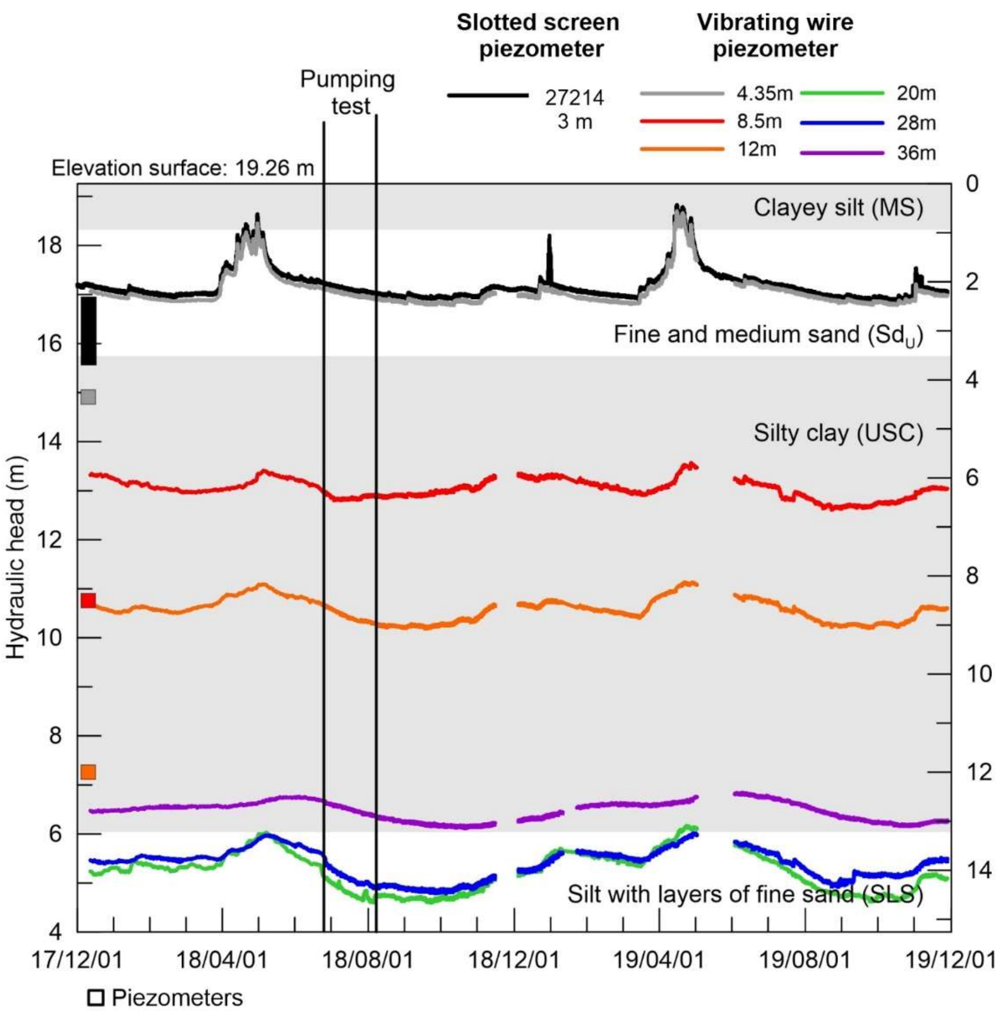

Figure 7. Hydraulic heads as a function of time for the VWPs and the slotted-screen piezometer located at the study site. Site stratigraphy is included for reference.

In order to compare the pressure variations at different depths, the difference in pore pressure (presented here as hydraulic head) since 1 January was computed annually for each piezometer (Figure 8). The data were then compared to river discharge variations measured at a gauging station on the Sainte-Anne river located approximately 50 km to the north. If groundwater dynamics at the field site were driven exclusively by meltwater infiltration and vertical flow, the hydraulic head data would show a reduction in the amplitude of the spring event with depth, along with a phase shift (see next section).

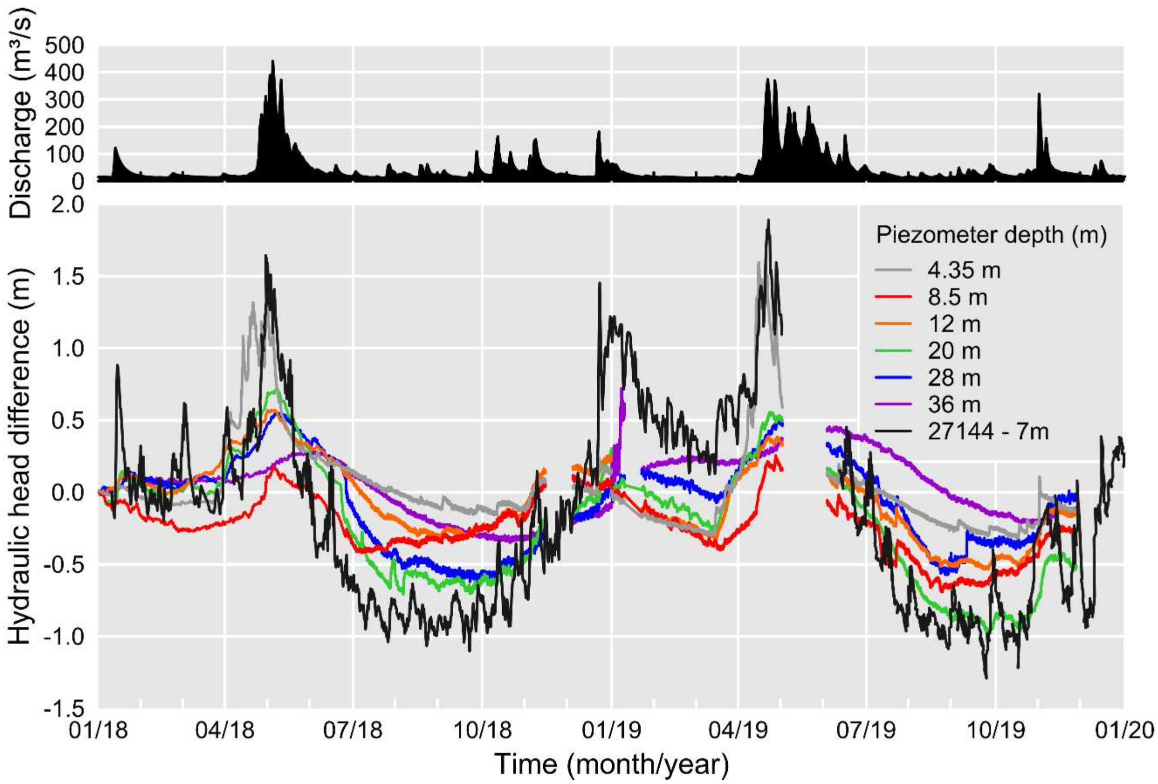

Figure 8. VWP pore pressure variations (presented as hydraulic head) and discharge within the Sainte-Anne river from 1 January 2018 to 1 January 2020 as a function of time.

The trend in Figure 8 does not support the assumption that groundwater flow on-site is exclusively vertical, as the piezometer located at a depth of 20 m has a head increase larger than piezometers above (8.5 and 12 m). Also, the piezometer located at 12 m depth shows a larger increase in head than the one at 8.5 m. Furthermore, the increases in head observed in the piezometers match well with increases in discharge measured within the river. Specifically, the increases in river discharge can help explain the increases in hydraulic head observed during late 2018 and early 2019, as the field site was covered by snow during this period, and the increase in head resulting from surface water infiltration would have been minimal. Together, these results indicate that groundwater dynamics at the site will not be adequately represented by a simple, 1-D vertical flow model.

4.3.1 Vertical flow simulations

The vertical flow model simulates the evolution of pore pressures in the silty clay layer resulting from the infiltration of precipitation and subsequent downward flow of groundwater. The hydraulic conductivity K_v of the silty clay layer varies from 4.5×10^{-10} to 1.1×10^{-9} m/s according to the triaxial cell tests, while the specific storage coefficient S_s, varies from 3.6×10^{-5} to 1.0×10^{-4} m^{-1} (Table 1). The ratio of these parameters gives a hydraulic diffusivity D varying from 4.5×10^{-6} to 3.1×10^{-5} m^2/s.

Simulation results for 4.35, 8.5 and 12 m depth illustrate what is expected following the infiltration of surface water: an increase in hydraulic head near the surface, followed by the attenuation of the pressure wave with depth (Figure 9). However, data from vibrating wire piezometers show a greater amplitude of the signal for hydraulic head at 8.5 m than at 12 m. For this specific simulation, the maximum D of $3.1 \text{x} 10^{-5}$ m^2/s was used to fit the 12 m curve, as both curves could not be fit together. Thus, results indicate that the variations in head (and pore pressure) observed on site cannot be adequately explained by infiltration alone. Note that the model assumes hydrostatic conditions, while a vertical downward gradient was observed at the site. This should not change the simulated trend, but it could impact the diffusivity values needed to fit the curves.

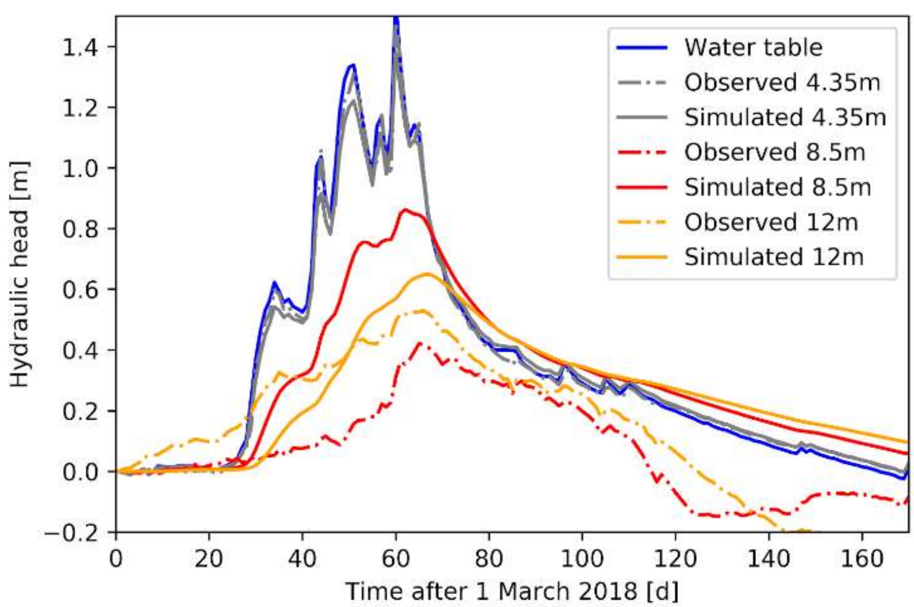

Figure 9. Simulation of hydraulic head variations in the USC unit resulting from surface water infiltration since March 1, 2018 (Location 27099). Note the poor agreement between the simulated and observed water levels at 8.5 m depth.

4.3.2 Lateral flow simulations and the influence of the Sainte-Anne River

The results in Section 4.2 indicate that infiltration from precipitation snowmelt cannot fully explain the variations in hydraulic head and pore pressure observed in the silty clay unit (USC). Given the proximity of the Sainte-Anne River (450 m northeast of the study site; Figure 2), it is possible that changes in river stage influence the pore pressures observed at the study site. For this to occur, unit Sd_L must be both continuous and in hydraulic connection with the river, which is the case here (Figure 3).

The second model simulation evaluated how a pressure wave would propagate horizontally through a hydraulically-connected sand layer as a result of an increase in river stage (Figure 7). The second simulation is able to broadly recreate the overall trends of the observed data, but the timing of the maximum head value, as well as the head recession, is not well captured by the model (Figure 10).

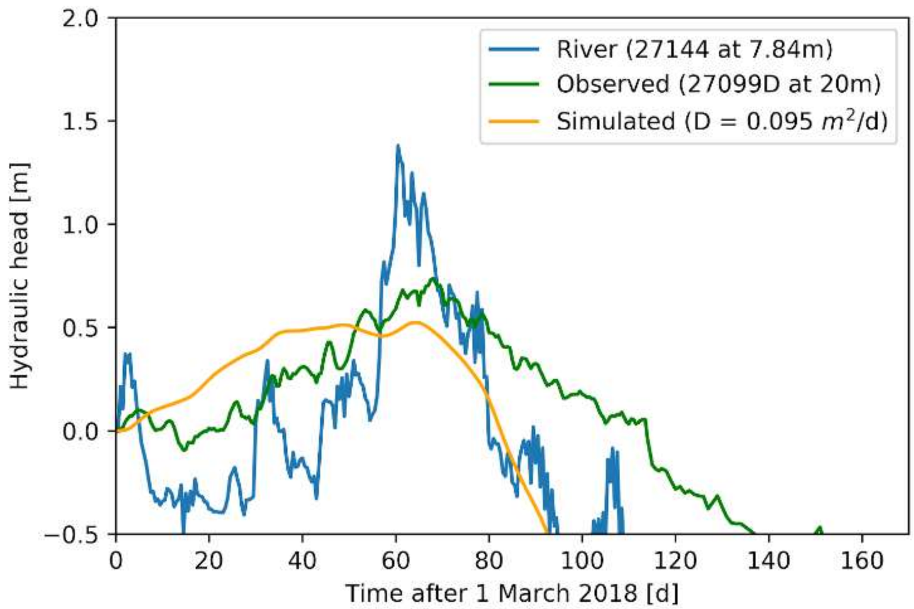

Figure 10. Hydraulic head variation in unit Sd_L (27099) as a function of time, resulting from variations in the stage of the Sainte-Anne River.

The results of the simple analytical solution used here suggest that other processes, in addition to horizontal flow, are responsible for the head variations observed at piezometer nest 27099. The simulated peak arrives about five days before the peak observed by the VWP, and the increase in head dissipates around the same time that the river stage recedes. Data from the VWP show that the recession in head values to the 0 m reference point takes about 25 days longer than the model predicts. Furthermore, this fit was obtained using a D value that is about two orders of magnitude smaller (0.095 m^2/d) than the D value that would be computed using the values from Table 1 (D = 2.75 m^2/d). This smaller value was the result of manually adjusting the S_s value until the best visual fit to the data was obtained, and the value used to produce the results in Figure 10 was 7.3 x 10^{-5} m^{-1}.

The fact that the hydrogeologic conditions do not perfectly match the assumptions of the analytical solution likely further contributes to the inability of the model to successfully recreate the data. The model utilized here assumes that the layer of fine sand (Sd_L, the lower aquifer on site) is confined and completely saturated, which is not entirely the case at the field site. While unit Sd_L appears to be confined by units SLS and USC, piezometer data indicate the presence of a phreatic water table. If the aquifer is unconfined, variations in the height of the water table will be governed by S_y as opposed to S_s, and the equation describing such fluctuations cannot be solved analytically. Therefore, the use of an analytical solution that can simulate partial/leaky confinement, such as the solution presented in Barlow et al., (2000), would likely yield better results. That said, the simulation in Figure 10 was able to broadly recreate the dynamics of the head variations while using a hydraulic diffusivity that reflects a S_s value that is only moderately larger than the one computed from the barometric compensation data. Thus, while it is likely that the Sainte-Anne river has an influence on the water level in the layer of fine sand, the combined influence of vertical flow and possible unconfined conditions make it difficult to characterize the extent of this influence without using numerical methods.

4.3.2 Groundwater Flow Directions

Horizontal hydraulic gradients and groundwater flow directions at the study site were calculated at various times between November 2017 and July 2019 using the 9 hydraulic piezometers (Figure 11). The average groundwater flow direction in unit Sd_U is 150°N, which corresponds to the slope of the terrain. The groundwater flow direction for unit T is about the same as for unit Sd_U. However, groundwater flow direction in unit Sd_L is slightly different than the other units, with groundwater flowing between 185 and 210°N.

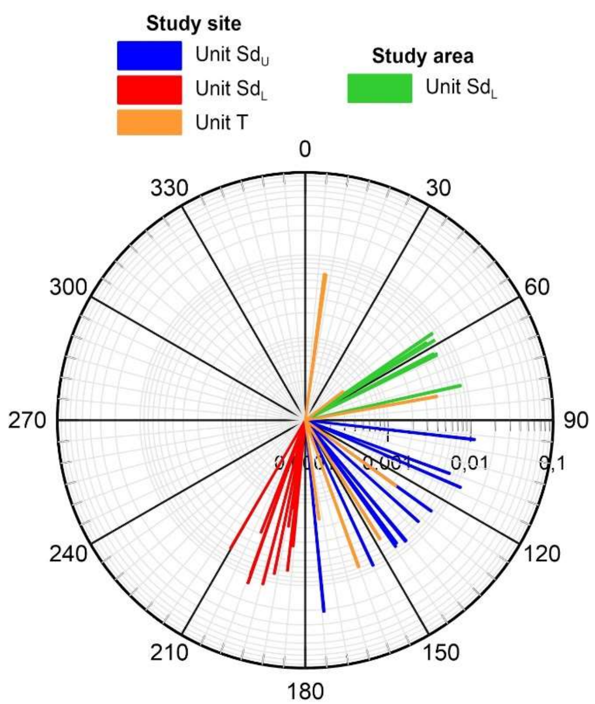

Figure 11. Groundwater flow direction and hydraulic gradient in units Sd_U, Sd_L and T measured at the study site and over the study area.

Regional groundwater flow direction over the study area was also computed for unit Sd_L using piezometers located at sites 27115, 27144 and 27099 (Figure 1b). It shows that groundwater flow direction for the Sd_L layer is toward northeast (47-77°N), with hydraulic heads higher at the study site than close to the Saint-Anne river. This direction is at an angle between 73-113 degrees of the flow directions found at the study site (150°N) for this unit.

5 Discussion

5.1 Seasonal infiltration dynamics

The elevation of the water table generally decreases during the summer months, however small, short-term increases in water table elevation are seen as a result of precipitation events. While the 5TM probes at the site show a rapid increase in water content after precipitation events, the high potential evapotranspiration (PET) during summer results in most of the precipitation returning to the atmosphere and only a small fraction infiltrating to become recharge. In the deeper parts of the unsaturated zone, water content variations have smaller, slower responses to precipitation events, and the groundwater flow dynamics are effectively controlled by the slow, diffuse flow occurring in the underlying silt unit (USC). However, large precipitation events (> 10 mm/d) provide sufficient infiltration to raise the elevation of the water table in the shallow aquifer (Figure 6). The rapid increases in water table elevation that occur after these events suggests that fractures or macropores are present in the silt. The observation of large-diameter (1-cm) worm holes during excavation of the instrumented trench further supports the theory that rapid water table rises on site are driven by preferential flow.

During the fall, frequent precipitation events cause the water table elevation to increase slightly. VWC also steadily increases during these months, with the surface probe (5TM-5, 0.1 m) indicating saturation. This increase in water table elevation is primarily driven by a reduction in surface evapotranspiration allowing for the infiltration of a greater quantity of water.

In winter, the daily air temperatures are mostly below freezing, precipitation is mainly in the form of snow, and the ground is frozen and covered with accumulated snowfall. During this period, the freezing front progressively advances to a maximum depth of 0.4 m, which occurs in February 2019 (Figure 6). Infiltration from early December to mid-April is limited, due primarily to snow cover and a lack of liquid precipitation. During this period, the water levels in the shallow aquifer and the water content in the soil gradually decrease.

Slight increases in the elevation of the water table do occur in winter. These water table rises are accompanied by an increase in the water content in the soil (e.g. January 12, 2018). The water source for both of these phenomena is likely snowmelt, driven by above-freezing air temperatures which occur on a few occasions during the winter season (Figure 6a). While temperature data show that the ground is frozen during these episodes, the water from melting snow still infiltrates and reaches the water table. This occurs because only a small fraction of the pore space contains frozen water, which allows unfrozen water to circulate in the soil. As a result, the limited infiltration seen on-site during the winter period is primarily due to a lack of meltwater. It is possible that the magnitude of recharge resulting from this process could progressively decrease during winter, as repeated melting events in the winter could cause the pores and macropores to progressively get clogged with ice (Mohammed et al. 2019).

The melting of accumulated snow during the spring corresponds with the largest infiltration event in a given year. Interestingly, in April, when water infiltration is at its peak, the frost front seems to extend deeper into the soil profile. It should be noted that the soil is not necessarily completely frozen when subsurface temperatures are exactly 0° C, as ice and water coexist at this temperature. Thus, since spring meltwater is very cold (~ 0 ° C), a momentary drop in soil temperature can therefore provide information on the timing of snowmelt infiltration. During the spring snowmelt event, VWC probes show a rapid increase in water content, with many probes reaching saturation. Furthermore, probes 5TM-1 (2 m) and 5TM-2 (1.75 m) are inundated by the rising water table. The spring snowmelt lasts for about a month. Once snowmelt ceases, subsurface temperatures quickly begin to rise. Water levels measured in the hydraulic wells increase over a period of a month after the end of the spring snowmelt, peaking in early May. Due to its magnitude, the spring snowmelt event has a large impact on pore pressures deeper in the sedimentary sequence.

5.2 How vertical flow and the Sainte-Anne River influence pore pressure at the study site

The evolution of pore pressures at the field site is characterized by a significant increase in spring due to the infiltration of snowmelt, followed by a gradual decrease over the summer and winter seasons. The impact of daily precipitation is minimal compared to the pressure increases created by the spring snowmelt, which results in the highest observed pore pressures. Results further show that while the infiltration-driven pore pressure increases in the spring greatly influence the pore pressure of the USC deposit, there is an observable time lag between water infiltration and the increase in pore pressure, a phenomenon that has been observed in other massive clay deposits (Timms and Acworth 2005). This lag is a result of infiltration not occurring instantaneously across all formations on site, as the pressure pulse due to surface infiltration diffuses downward slowly. As a result, the hydrogeological properties of the individual layers on site will influence the propagation of the pressure wave resulting from infiltration, primarily through differences in hydraulic diffusivity (Van der Kamp and Maathius 1991). Data indicate that changes in hydraulic head propagate faster in sandy layers, where hydraulic conductivity is higher and compressibility is lower, than in clay layers that are less permeable and more compressible. Thus, in the greater context of the St. Lawrence Valley, the rate at which pore pressures increase depends on the hydrogeological properties of the materials at a given field site.

When 1-D models of the site were created to examine the influence of the spring infiltration on site water levels, simulation results showed that the hydraulic head will always decrease as a function of the depth. These results, however, are not supported by data from the vibrating-wire piezometers, which show that the hydraulic head at the base of the massive clay layer (USC; 12 m deep), is greater than observed at 8.5 m depth. This increase therefore cannot be explained solely by vertical flow from the surface.

When a hydraulic connection between the Sainte-Anne river and unit Sd_L was considered, the model successfully matched the timing of the maximum hydraulic heads and approximated the dynamics of the hydraulic head rise on site. However, the results did not demonstrate good agreement with the recession in head values which occur later in the year. These results suggest that changes in the stage of the Sainte-Anne River have some impact on the variations in pore pressures in the fine sand layer, however determining the exact extent of the influence of the river is beyond the capability of a relatively simple 1-D analytical solution. Thus, while these results suggest that the influence of a stream can travel over fairly long distances, determining the exact extent to which the river influences local pore pressures on site will require the use of more sophisticated 2- or 3-D numerical models.

It is perhaps unsurprising that neither simulation perfectly recreated the groundwater dynamics of the field site, as the relatively simple conceptual models utilized by these simulations did not adequately describe geologic complexity of the study location. In both simulations, the decrease in hydraulic head after the spring peak occurred faster than what was observed with the vibrating-wire piezometers. Even when different values of diffusivity D were used, it was not possible to obtain a better match between the simulated and observed values. Thus, other flow processes, which are not shown in the model, likely have an impact on the values measured by the vibrating-wire piezometer.

The complexity of the hydrogeological setting on site, which may include a second phreatic surface at depth, made it difficult to model the local groundwater dynamics using simple 1-D analytical models. Further complexity may have also been introduced by the stratigraphic dip of coarse-grained units that were in hydraulic connection with the river. Because of the orientation unit SLS/Sd_L, it is possible that it is easier for a pressure signal to propagate out of the river than it is for return flow to re-enter the river during periods of lower flow. Also contributing to this uncertainty is the fact that the variations in the level of the river are approximate. Thus, to better quantify the contributions of different processes to the observed groundwater dynamics at the field site, the authors recommend either using a more sophisticated analytical solution designed for complex river-aquifer interactions, or the use of a 2- or 3-D numerical model. Finally, the inclusion of observed variations in the stage of the Sainte-Anne river could assist in reducing the uncertainty of model predictions.

5.3 Site Conceptual Model

A detailed conceptual model was created to synthesize the geologic, hydrogeologic, and geotechnical data collected within the framework of this project (Figure 12). The conceptual model is based on the geological cross section, over which hydrogeological conditions are shown. The two water tables (phreatic surfaces) are shown based on hydraulic heads from the VWP. The minimum and maximum values for the year 2018 were used to determine maximum and minimum water table elevations (Figure 12).

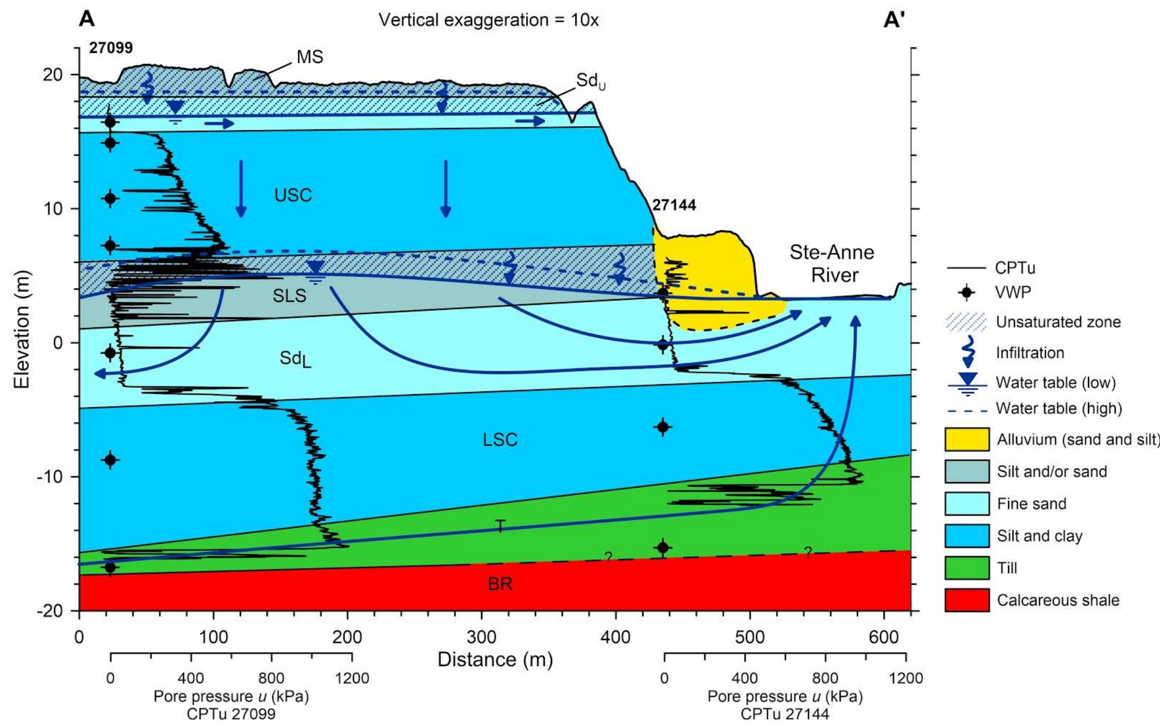

Figure 12. Conceptual model of the groundwater flow at Sainte-Anne-de-la-Pérade, along a profile A-A' between Locations 27099 and 27144.

The Sd_U unit forms an unconfined aquifer where the water table elevation varies by about 1.5 m annually. The direction of groundwater flow in this unit is highly variable and is likely influenced by local topography, ditches, and small streams.

Just below the unit Sd_U, a low permeability silty clay unit (USC) acts as an aquitard. There is a high vertical hydraulic gradient within this unit of about 0.65 m/m. The presence of this vertical gradient may explain the leaching of this unit, where a low pore-water salinity of 0.2 g/L was measured (Figure 2).

Just below unit USC, the sandy SLS and Sd_L units may be considered a deep unconfined aquifer. Analysis of the hydraulic gradient and dynamic pore pressure data show that there are two different flow systems on site, separated by a thin unsaturated zone that exists on the boundary of units USC and SLS (Figure 13). The unsaturated zone location could be determined by extending the hydrostatic profile from the lowest piezometers up to than elevation (z) of 5 m, using the CPTu profile as a guide (Figure 13 - right panel). At this point, the pressure line moves into the negative pressure zone, until it increases again to reach the positive values in the USC unit. This unsaturated zone would explain why the pumping test in the Sd_L unit did not introduce any drawdown in the USC unit above. However, as could be seen in Figure 7, the water table in this unit sometimes reaches the USC unit (mostly during spring). During these periods, it is likely that no unsaturated zone would exist. It should also be mentioned that this negative pressure zone may not me unsaturated, depending on the suction and the air entry pressure.

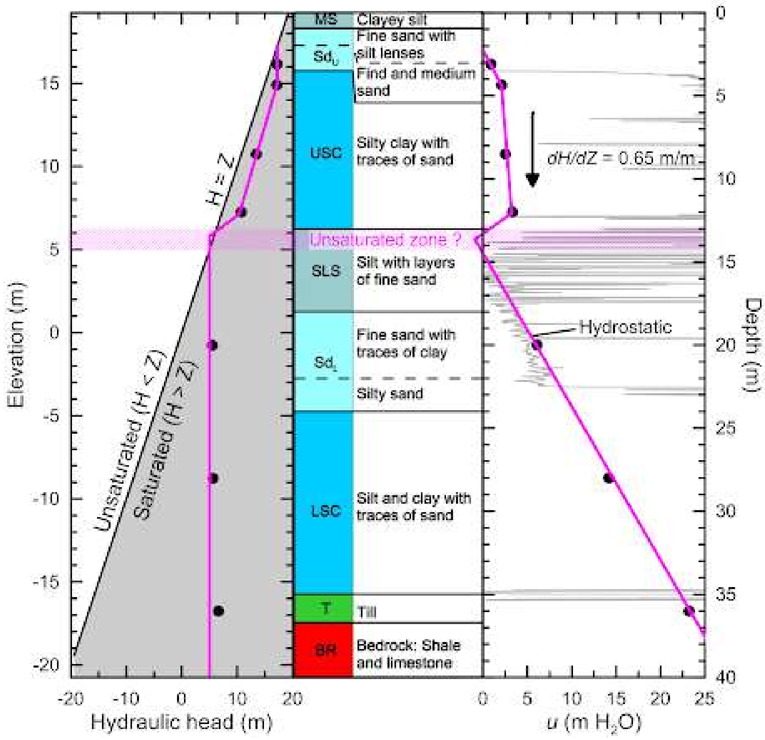

Figure 13. Hydraulic gradients profiles, stratigraphy, and dynamic pore pressure values as a function of depth. Black dots represent measurement points. The purple line is used to show the two different flow regimes present on-site: downward flow exists in the upper 14m of the section, while flow is largely hydrostatic at depths of 15m and below.

The clay unit USC most likely drains into unit SLS, an assertion supported by the direction of the hydraulic gradient at this location. The elevation of the water table in units Sd_U and SLS varies according to seasonal variations in the stage of the Sainte-Anne river. Field data show that the elevation of the water table in these deeper units fluctuates between 2-3 m seasonally. The maximum level of hydraulic head recorded at Location 27144 occurs in tandem with the maximum stage of the river, while the resulting pressure wave reaches Location 27099 a few days later. The recession of the hydraulic head on site took longer to propagate: the hydraulic head at Location 27099 reaches its minimum (coinciding with minimum river stage) in August, however the effects were not felt at Location 27144 until September.

Regardless of the time of year, the hydraulic head in the SD_L unit is higher at the study site than in the river, suggesting a flow of groundwater from the site to the river. However, groundwater flow direction measurements in the three screened piezometers at the study site suggest that the flow direction is toward the southwest. To reconcile these two observations, the phreatic surface in this layer of sand is represented in the form of a mound whose direction of flow is in these two directions. This is consistent with the hydrogeological context where a low permeability layer provides vertical recharge to an unconfined aquifer.

In the T and LSC units, just below unit Sd_L, the vertical hydraulic gradient is upward, but very low. This low vertical gradient combined with the low permeability of unit LSC likely explains why leaching was less extensive than what was observed in unit USC, and further explains why the pore-water salinity is closer to sea water. Horizontal flow is assumed in the medium permeability till unit towards the Sainte-Anne river, based on the hydraulic heads from the VWP (27099, 27144).

While simulation results were able to explain the dynamic behavior of the shallow and deep vibrating-wire piezometers, the behavior of the 8.5 and 12 m piezometers at the base of the clay layer requires additional study. Field data and simulation results appear to indicate that these piezometers are affected by both the surface water supply and the Sainte-Anne river. Meanwhile, the fact that the layer directly below (Sd_U) is not completely saturated is an additional complicating factor. The link between all of these conditions has not yet been investigated, and further analysis is necessary to better explain the observed site dynamics and determine the direction of groundwater flow at this location. Also, no hydraulic properties could be obtained for the SLS unit due to a lack of instrumentation. Since it is very heterogeneous and located at a key position in the hydrostratigraphic sequence, its role in the hydrogeology of the area could be critical, but remains uncertain. The use of more sophisticated 2D numerical models could greatly improve our understanding of the groundwater dynamics on site, and could assist in further refining the conceptual model presented here. For instance, a flow simulation considering the effect of the river and the seasonal variations of the water table in the surface aquifer would make it possible to better understand the dynamics of the flow in the clay layer.

5.4 Implications for Slope Stability

The data provided by the instrumentation at the Sainte-Anne-de-la-Pérade field site makes it possible to discuss the local potential for landslides in the massive clay units present on site. Landslide risk depends on several factors, such as the type of deposit present and its physical properties, as well as the mechanical and hydrogeological conditions found on site. It also depends on external factors, such as climate or nearby anthropogenic modifications (Lafleur and Lefebvre 1980; Leroueil et al. 1983; Leroueil 2001). In this study, the pore pressures in clay deposit and their associated hydraulic gradients were used to assess slope stability.

For limit-equilibrium stability analysis in Champlain Sea deposits in Quebec, a relatively simple stratigraphic sequence is usually considered in practice: one where the low permeability Champlain clay deposits are bounded above and below by more permeable layers (Lafleur and Lefebvre 1980; Lefebvre 1986, Lefebvre 2017). The lower layer is often represented as till or fractured bedrock, while the upper layer is either made of alluvial/littoral sand, or fractured, desiccated, and oxidized clay crust. This simple stratigraphic sequence is commonly assumed because it is often appropriate for use in in Champlain Sea deposits (Lefebvre 2017). As shown here, a simplified representation of the groundwater flow system may not apply when a “drain layer” exists within a slope that borders a river, as the results of this study indicate that flow on site is likely two dimensional. In such a case, a more detailed hydrogeological analysis (like the one presented here) may be required in order to fully characterize the local groundwater flow system and assess its impact on slope stability.

The conceptual model of the groundwater flow system present on site shows that the layer of silty clay (USC), which functions as an aquitard that separates the upper and lower aquifers, is not continuous over the area of investigation. This layer has been eroded away by downcutting in the river valley, resulting in the exposure of the alternating clay-silt and fine sand layer (SLS) near the base of the slope (Figure 12). Results further indicate that this layer (SLS) is not completely saturated. It is therefore possible that unit USC drains into the underlying, more permeable unit SLS. Due to the presence of this "drain layer," pore pressures in the silty clay are able to remain relatively low, which is more favorable to stability than in a slope totally constituted of clay and without this "drain layer". The presence of a downward gradient in the SLS and Sd_L units at the foot of the slope further promotes stability in the clay layer. The combination of these conditions leads to an increase in effective stresses; and, at the same time, an increase in the shear strength and in stability.

Future work should use 2-D transient flow simulations or more sophisticated analytical solutions to represent groundwater flow in the slope near the river and calculate the corresponding safety coefficient. In addition, an even more in-depth soil stability study that includes the physical properties and mechanical conditions of the soil layers present would also be beneficial for continued site management.

Previous work has shown that pore pressures in the soil are highest during the Spring, due to increased precipitation and/or snowmelt-derived infiltration (Cloutier et al. 2017). However, changing climatic conditions are likely to alter several key parameters used in the forecasting of landslide hazards, namely precipitation, the extent and thickness of snow cover, wind speed, and the number and timing of zero-degree days (Comenga et al. 2013). As a result, it is recommended that site monitoring be increased at the study site, particularly from April to June, in order to gain a better understanding of site dynamics and to better predict landslides in the area.

The data presented here demonstrate the importance of high-frequency pore pressure monitoring. In this study, such monitoring was able to capture the transient dynamics of the local groundwater flow system, which were significantly different than the simple flow conditions that are commonly assumed (Lafleur and Lefebvre 1978; Lafleur and Lefebvre 1980; Lefebvre 1986). In addition, this study shows the value of considering regional hydrological conditions when analysing local seepage and pore pressure variations, as this broader context was essential for understanding the seasonal variations in the local hydrological regime.

6 Conclusion

This study sought to acquire data with high spatial and temporal resolution in order to better understand the seasonal variations in hydrogeological conditions in a succession of complex marine deposits. These results were then integrated into a conceptual model that describes the mechanisms responsible for pore pressure variations at different locations within the stratigraphic sequence. The resulting conceptual model details a groundwater flow system which is significantly more complex than the more commonly used model which considers a homogeneous flow system for slope stability in sensitive clays (Lefebvre 1986). Variations in the water table that occur in the layer of fine to medium sand located near the surface (Sd_U) propagate into the underlying silty clay layer (USC). However, due to the low hydraulic conductivity and the high compressibility of unit USC, these variations do not propagate very deeply, and are strongly attenuated. The significant variations in pore pressures measured in the underlying sand layers (a combination of units SLS and Sd_L), are likely partially attributable to variations in the water level in the nearby Sainte-Anne river. The high contrast in hydraulic conductivity between the sand layers and the overlying silty clay means that the layer of fine sand is not completely saturated and contains a second phreatic surface. Finally, the Sainte-Anne river also influences pore pressures in the underlying silt and clay layer and possibly in the silty clay layer above. As such, the conceptual model illustrates that the flow of groundwater at the study site is complex and determined by (i) the highly-heterogeneous nature of the geological materials present on site, (ii) the contrasting hydraulic and geotechnical properties of these materials, (iii) the presence of two unconfined aquifers on site, one surficial and one at depth, and (iv), the presence of the Sainte-Anne River. While the hydrogeological context is quite unique, it may be found elsewhere in the St. Lawrence Lowlands.

The presence of the units SLS and Sd_U have a relatively beneficial effect on the stability of the slopes near the river. These layers act as a horizontal drain that relieves excess pressure within the massive clay layer (USC). The presence of this drain layer, as well as the fact that the clay mass does not extend to the base of the slope, results in the formation of a constant downward hydraulic gradient between the two layers. This downward gradient serves to increase both the effective stresses and the shear strength of unit USC, decreasing the risk of a landslide on site. However, this reduced landslide risk is highly-site specific, and occurs only as a result of the unique hydrogeological setting.

Future work at the Sainte-Anne-de-la-Pérade site should focus on monitoring the stage of the Sainte-Anne river near the study site, which would allow for more accurate and in-depth investigations of pore pressure variations at depth. Furthermore, additional surveys with the CPTu piezocone and the drilling of boreholes between the study site and the Sainte-Anne river would make it possible to more precisely assess the continuity of the layers at depth and monitor the horizontal distribution of pore pressures. The hydraulic properties of the SLS unit should also be measured, since it likely has a key role in the hydrogeology of the area. Additional 2D digital simulations could be carried out in order to combine the impact of surface water infiltration, variations in the level of the Sainte-Anne river and the presence of an unsaturated zone under the massive clay deposit. These simulations would make it possible to obtain results similar to what is observed by vibrating-wire piezometers in the silty clay layer. Additional understanding of these processes would make it possible to develop a numerical model that is more representative of the local site conditions. Such a model could be used to make long-term hazard predictions that consider a number of different climate change scenarios.

Acknowledgements

This work was funded by the Quebec Ministry of Public Security through the 2013-2020 Action Plan on Climate Change (PACC 2013-2020) and the Québec Government's Green Fund. Christopher Neville is thanked for providing derivation of Equation 7. Quebec Ministry of Transportation is thanked for carrying out the borings and soundings, and for the permission to use the data. Martin d’Anjou from the Quebec Ministry of Transportation is also thanked for his critical help in the field. Finally, the authors would also like to thank the two anonymous reviewers whose input greatly improved this manuscript.

References

ASTM D5084-16a. 2016. Standard Test Methods for Measurement of hydraulic conductivity of saturated porous materials using a flexible wall permeameter. ASTM international.

Bouwer, H. and Rice R.C. 1976. A slug test for determining hydraulic conductivity of unconfined aquifers with completely or partially penetrating wells. U.S. Water Conservation Laboratory, Agricultural Research Service, U.S. Department of Agriculture, Phoenix, Arizona, **12**(3): 423-428.

Boyle S., Karlsrud K., Hoydal O.A. 2009. Pore-pressure response in a marine clay slope in southeast Norway. Can. Geotech. J., **46**: 1391-1405.

CAN/BNQ 2501-110. 2006. Sols – Détermination de la résistance au cisaillement non drain et de la sensibilité des sols cohérents à l’aide du pénétromètre à cône suédois. Conseil Canadien des Normes - Bureau de normalisation du Québec.

CAN/BNQ 2501-025. 2013. Sols – Analyse granulométrique des sols inorganiques. Conseil Canadien des Normes – Bureau de normalisation du Québec.

Cloutier, C., Locat, J., Geertsema, M., Jakob, M., and Schnorbus, M. 2016. Potential impacts of climate change on landslides occurrence in Canada. In Slope Safety Preparedness for Impact of Climate Change. *Edited by* Ho, K., Lacasse, S., and Picarelli, L. pp. 73-103. CRC Press. Boca Raton, Fl.

Cloutier, C., Locat P., Demers, D., Fortin, A., Locat, J., Leroueil, S., Locat, A., Lemieux, J.-M. and Bilodeau, C. 2017. Chapter 47 – Development of a long term monitoring network of sensitive clay slopes in Québec in the context of climate change. *In* Landslides in Sensitive Clays - From Research to Implementation Advances. *Edited by* Thakur, V., L’Heureaux, J.S., and Locat, A. pp. 549-558. Springer, Dordrecht

Comegna, L., Picarelli L., Bucchignani, E. and Mercogliano, P. 2013. Potential effects of incoming climate changes on the behavior of slow active landslide in clay. In *Landslides 2013*, pp. 373-391. Springer, Dordrecht

Cooper, H.H., Bredehoeft J.D. and Papadopulos S.S. 1967. Response of a finite-diameter well to an instantaneous charge of water. Water Resources Research, **3**(1): 263-269.

Diène, M. 1989. Mesure *in situ* de la perméabilité des argiles. Thèse de doctorat. Département de génie civil, Université Laval.

Demers, D., and Leroueil, S. 2002. Evaluation of preconsolidation pressure and the overconsolidation ratio from piezocone tests of clay deposits in Quebec. Canadian Geotechnical Journal. **39**: 174-192.

Demers, D., Robitaille D., Potvin J., Bilodeau C., Dupuis C. 2008. La gestion des risques de glissements de terrain dans les sols argileux au Québec. In : J. Locat, D. Perret, D. Turmel, D. Demers et S. Leroueil, (2008), Comptes rendus de la 4e Conférence canadienne sur les géorisques: des causes à la gestion, Presse de l'Université Laval, Québec, p. 519-526.

Demers, D., Robitaille, D., Locat, P., and Potvin, J. 2014. Inventory of large landslides in sensitive clay in the province of Québec, Canada: Preliminary analysis. *In* Landslides in Sensitive Clays. *Edited by* L'Heureux, J-S., Locat, A., Leroueil, S., Demers, D., Locat, J. Advances in Natural and Technological Hazards Research, vol 36. Springer, Dordrecht

Fortier, P., Germain, A., Kokutse, N. and Lemieux, J.-M. 2018. Rapport d'essais de perméabilité à charge variable. Rapport d'étape 02. Rapport-PACC-17-18-06-02. Projet PACC-17-18-06. Département de géologie et de génie géologique, Université Laval, p. 19.

Freeze, R.A., and Cherry J.A. 1979. Groundwater. Prentice Hall, Englewood Cliffs, N.J.

Gauthier, D., and Hutchinson, D. J. 2012. Evaluation of potential meteorological triggers of large landslides in sensitive glaciomarine clay, eastern Canada. Natural Hazards & Earth System Sciences, **12**(11).

Hungr, O and Locat, J. 2015. Examples of common landslide types in Canada: Canadian technical guidelines and best practices related to landslides: a national initiative for loss reduction. Geological Survey of Canada Open File 7897.

Jarrett, P.M., and Eden, W.J., 1970. Groundwater flow in eastern Canada. Can. Geotech. J., **7**: 326-333.

Kelly, R.B. Pineda, J.A., Bates, L., Suwal, L.P., and Fitzallen, F. 2017. Site characterization for the Ballina field testing facility. Géotechnique **67**(4): 279-300.

L'Heureux, J-S., Locat, A, Leroueil, S. Demers, D. and Locat, J. 2014 Landslides in Sensitive Clays - From Geosciences to Risk Management. *In* Landslides in Sensitive Clays - From Geosciences to Risk Management. *Edited by* L'Heureux, J-S., Locat, A, Leroueil, S. Demers, D. and Locat, J. p. 1-9 Springer, Dordrecht

Lafleur, J., and Lefebvre, G. 1978 Influence des écoulements souterrains sur la stabilité des pentes naturelles d'argile. Ministère des richesses naturelles, Direction générale des mines, Direction de la géologie, Service de géotechnique. Québec, Canada.

Lafleur, J., and Lefebvre, G. 1980. Groundwater regime associated with slope stability in Champlain clay deposits. Can. Geotech. J., **17**(1): 44-53.

Lefebvre, G. 1986. Slope instability and valley formation in Canadian soft clay deposits. Can. Geotech. J., , **23**(3): 261-270.

Lefebvre, G. 1996. Soft sensitive clays - Chapter 24. *In* Landslides: investigation and mitigation, *Edited by* K. Turner and R.L. Schuster; Transportation Research Board, Special Report 247, p. 607- 619.

Lefebvre, G. 2017. Sensitive clays of Eastern Canada: from geology to slope stability. *In* Landslides in Sensitive Clays - From Research to Implementation Advances. *Edited by* Thakur, V., L'Heureaux, J.S., and Locat, A. pp. 15-34. Springer, Dordrecht

Leroueil, S., Tavenas, F., and Bihan, J. P. L. 1983. Propriétés caractéristiques des argiles de l'est du Canada. Can. Geotech. J., **20**(4), 681-705.

Leroueil, S. 2001. Natural slopes and cuts: movement and failure mechanisms. Geotechnique, **51**(3): 197-243.

Locat, J., Lefebvre, G., and Ballivy, G. 1984. Mineralogy, chemistry, and physical properties interrelationships of some sensitive clays from Eastern Canada. Can. Geotech. J., **21**: 530-540.

Locat, J. 1996. On the development of microstructure in collapsible soils: lessons from the study of recent sediments and artificial cementation. *In* Genesis and Properties of Collapsible Soils *Edited by* Derbyshire, E., Dijstra, T., and Smalley, I.J. Klewer Academic Publisher, Dordrecht. pp. 93–128.

Locat, J., Tanaka, H., Tan, T.S., Dasari, G.R. and Lee, H. 2003. Natural soils: geotechnical behavior and geological knowledge. *In: Characterisation and Engineering Properties of Natural soils*. Tan et al., ed., Sweeta and Zeitlinger, Lisse, Publisher, pp.: 3-28.

Locat, J. 2011. La localisation et la magnitude du séisme du 5 février 1663 (Charlevoix) revues à l'aide des mouvements de terrain. Can. Geotech. J., **48**: 1266-1286.

Locat, A., Demers, D., Locat, P., Geertsema, M. 2017. Sensitive Clay Landslide in Canada. 70th Can. Geotech. Conf. (GeoOttawa2017), 8p.

Marefat, V., Duhaime F. and Chapuis R.P. 2015. Pore pressure response to barometric pressure change in Champlain clay: Prediction of the clay elastic properties. Engineering Geology, **198**: 16-29.

Moench, A.F., and Barlow, P.M. 2000. Aquifer response to stream-stage and recharge variations. I. Analytical step-response functions. J. Hydrol., **230**: 192-210. DOI: 10.1016/S0022-1694(00)00175-X

Mohammed, A., Pavlovskii, I., Cey, E. and Hayashi, M. 2019. Effects of preferential flow on snowmelt partitioning and groundwater recharge in frozen soils. Hydrology and Earth System Sciences, **23**. DOI: 10.5194/hess-23-5017-2019

Parent, M. and Occhietti, S. 1988. Late Wisconsinan Deglaciation and Champlain Sea Invasion in the St. Lawrence Valley, Québec. Géographie physique et Quaternaire, **42**(3) : 215–246. https://doi.org/10.7202/032734ar

Quigley, R.M. 1980. Geology, mineralogy, and geochemistry of Canadian soft soils: a geotechnical perspective. Can. Geotech J., **17**: 261–285.

Rosenberg P., Provençal J., Lefebvre G., Paré J.-J. 1985. Influence of the groundwater on the stability on a clay bank in Baie James, Québec. Can. Geotech. J., **22**: 409-413.

Tavenas, F. 1984. Landslides in Canadian Sensitive Clays - A State-of-the-Art. 4th International Symposium on Landslides, Toronto, 1: 141-153.

Tavenas, F., Jean, P., Leblond, P., and Leroueil, S. 1983. The permeability of natural soft clays. Part II: Permeability characteristics. Can Geotech J., **20**(4), 645-660.

Timms, W. A., and Acworth, R.I. 2005. Propagation of pressure changes through thick clay sequences: an example from Liverpool Plains, NSW, Australia. Hydrogeology Journal, **13**:858-870. https://doi.org/10.1007/s10040-005-0436-7

Tipman, J., Barbour L. and Van der Kamp G. 2017. An evaluation of methods to remove barometric effects from pore pressure data. University of Saskatchewan. Canada. 70th Can. Geotech. Conf. (GeoOttawa 2017), 8 p.

Torrance, J.K. 1975. On the role of chemistry in the development and behavior of the sensitive clays of Canada and Scandinavia. Canadian Geotechnical Journal, **12**: 326-335.

Uhlemann, S., Smith, A., Chambers, J., Dixon, N., Dijkstra, T., Haslam, E., Meldrum, P., Merritt, A., Gunn, D., and Mackay, J. 2016. Assessment of ground-based monitoring techniques applied to landslide investigations. Geomorphology, **253**: 438-451.

Van der Kamp, G., and Maathuis, H. 1991 Annual fluctuations of groundwater levels as a result of loading by surface moisture. J. Hydrol., **127**: 137–152.